THE JOURNAL OF PHYSICAL CHEMISTRY C

Article

pubs.acs.org/JPCC

In-Silico Design of a Donor−Antenna−Acceptor Supramolecular Complex for Photoinduced Charge Separation

Adriano Monti, Huub J. M. de Groot, and Francesco Buda*

Leiden Institute of Chemistry, Leiden University, Einsteinweg 55, 2300 RA Leiden, The Netherlands

Supporting Information

ABSTRACT: We investigate via density functional theory a series of donor−antenna−acceptor molecular rectifiers designed as modules for artificial photosynthesis devices. We consider triad modules containing phenothiazine (PTZ) as the electron donor and different derivatives of naphthalene diimide (NDI) as the antenna and secondary electron acceptor. The choice of the molecular components in the triad is guided by the redox and optical properties of each subunit. Using time-dependent DFT in combination with the long-range corrected xc-functional CAM-B3LYP we investigate how photoinduced charge transfer states are affected by systematic modifications of the triad molecular structure. In particular, we show how by controlling the length of the molecular bridges connecting the different charge separator subunits it is possible to control the driving force for the relaxation of the excitonic state into the full charge-separated state. On the basis of these findings we propose a supramolecular triad consisting of inexpensive and readily available molecular components that can find its implementation in artificial devices for solar energy transduction.

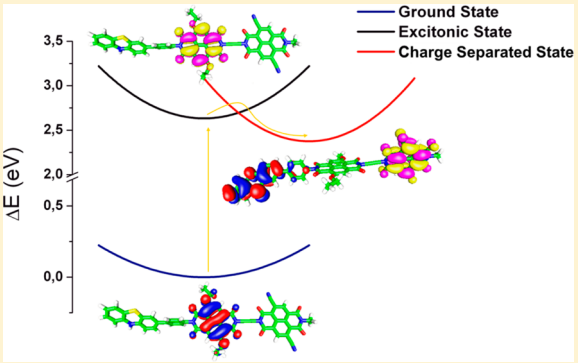

1. INTRODUCTION

Progress in the design and synthesis of nanodevices for artificial photosynthesis can be strongly supported by computational modeling methods able to predict optimal target properties for light energy conversion in the computer prior to the realization in chemical laboratories.[1−5] A very primary target is to achieve a long-lasting charge-separated state for dye-sensitized solar cells and artificial photosynthesis applications.[6−9]

Despite the great improvements in the sunlight-to-photocurrent conversion rates achieved by modern devices, their efficiency is still largely affected by the occurrence of charge recombination. Recent publications suggest that efficient charge separation can be realized only by systems composed of three or more subunits arranged in a Donor−Antenna−Acceptor (D−An−A) like design, presenting an optimized energy gradient and electronic coupling.[10−13]

Our goal here is to use density functional theory (DFT) based methods to optimize the optical and electronic properties of a molecular system designed for photoelectrochemical applications prior to its experimental realization. The aim is to obtain a photosensitive triad-like charge separator for photocatalytic and photovoltaic applications which shows ultrafast unidirectional electron transfer leading to the formation of a charge-separated state (CS) sufficiently stable to kinetically allow redox reactions at the donor (D) and the acceptor (A) moieties.[14] We chose the triad components on the basis of their ground and excited state redox potentials to obtain negative potential energy gradients between the donor−antenna and the antenna−acceptor subunits. Furthermore, the donor and the acceptor are chosen considering the potential boundaries necessary to couple the proposed triad within a device employing a silicon electrode and a commonly used electrolyte, such as iodide/triiodide.[15]

By systematically changing the connections between the donor, the antenna, and the acceptor, we highlight how structural modification can be used to control the relative energies and electronic couplings between different excited states. In this way we are able to design a molecular triad for which the photoexcitation of the antenna will trigger redox processes resulting into the formation of a final D^+−An−A^- charge-separated state.

The presence of the antenna complex between the donor and the acceptor should induce a considerable tunneling barrier for charge recombination and consequently reduce the electronic coupling between the charge-separated and ground states of the triad. This will resolve in delaying the electronic recombination to the state of minimal energy and increase the lifetime of the CS.

The molecular components used in this study as donor, antenna, and acceptor are, respectively, the 10,10a-dihydro-4aH-phenothiazine (PTZ), the 2,6-diethoxy-1,4,5,8-diimidenaphthalene (NDI_1), and the 2,6-dicarbonitrile-1,4,5,8-diimidenaphthalene (NDI_2). A schematic representation of the single components and of the different complexes analyzed is reported in Figure 1.

Individually, PTZ, NDI_1, and NDI_2 have already been discussed in the literature and are well-known for their robustness and ease of synthesis. They have been chosen based on the perfect match between their well-characterized optical and

Received: May 23, 2014
Published: June 30, 2014

   dx.doi.org/10.1021/jp505105a | J. Phys. Chem. C 2014, 118, 15600−15609

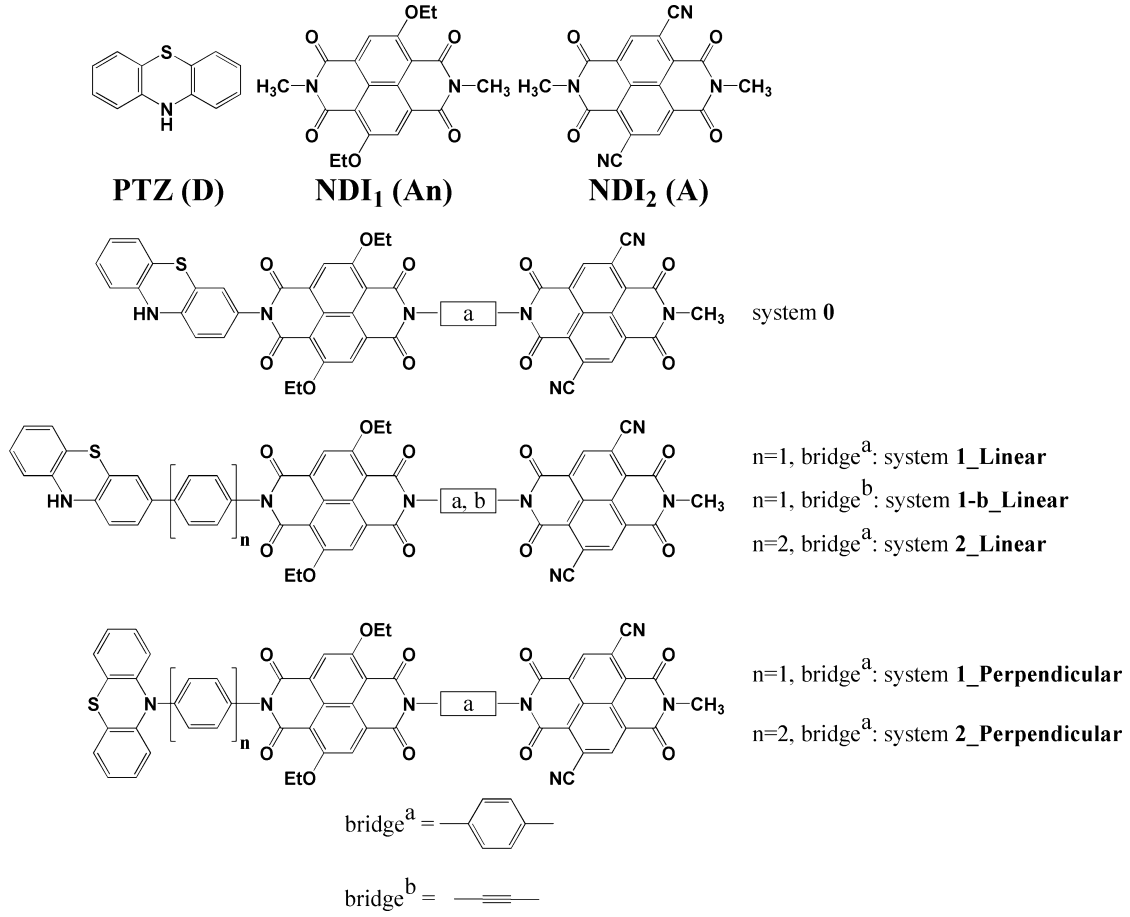

Figure 1. Molecular structures of the studied compounds. PTZ acts as the electron donor (D), NDI_1 as the antenna (An), and NDI_2 as an electron acceptor (A). The number of phenyl units between the D and An is indicated with *n*. Two different bridges (a and b) between the An and A are considered. Linear and perpendicular refer to the relative arrangements of PTZ and the phenyl bridge.

electronic properties and the device requirements. The members of the naphthalene diimide family form an important class of chromophores which has been extensively analyzed in recent years and applied in a wide range of devices, such as supramolecular switches, chemosensors, n-type semiconductors in organic transistors, light-harvesting chromophores in dye-sensitized solar cell (DSSC), and electron acceptors in photoactivated artificial charge separators.[8,16−19] The versatility of these compounds is due to their peculiar electronic properties that can be easily tuned through a selective functionalization of the naphthalene core.[20] By choosing the appropriate functional groups it is possible to adjust the HOMO and LUMO orbital energies and their relative gaps. This allows us to control the molecular absorption range and to adapt the molecular redox properties with respect to the environment requirements.

As shown by Sakai et al.[20] due to their different functionalization NDI_1 and NDI_2 present absorptions in two different regions of the incoming photon spectrum. While the first is photoactive also into the visible, the second shows activity only in the UV region. This ensures NDI_1 to be the only active chromophore for applications with visible light in solar energy conversion. On the other hand, NDI_2 is chosen not only for its absorption properties but also for its characteristic ability to form stable anionic radicals.[21] Especially in a context where several molecules are bound together through $\pi-\pi$ stacking, NDI_2 has been shown to behave as an n-type semiconductor material.[22] This characteristic makes it a very good candidate as an electron acceptor able to increase the electron−hole distance through electron delocalization thus decreasing the probability of its recombination into the ground state. Additionally, the LUMO energy of NDI_2 aligns well with the valence band of silicon, opening the possibility of establishing a p−n junction between the electron rectifier and a silicon-based electrode.

Finally, phenothiazine is a strong reducing agent photoactive only in the UV region that is already widely employed as pesticide and in pharmaceutical or optical applications.[21,23,24] Thanks to the strong interaction between the $2p_z$ electrons of the nitrogen atom of the central heterocyclic ring with the peripheral benzenes, PTZ can easily form cation-radical species and stabilize them through resonance delocalization of the positive charge into those electron-rich moieties.[23] PTZ is therefore an optimal electron donor able to quench the hole created in the antenna upon photoexcitation.

Herein we compare a series of molecular triads designed for photoinduced unidirectional charge separation. The donor−antenna distance is proved to be a key parameter to control the relative energies of different excited state potential energy surfaces (PESs). It is shown that it is possible to induce the concerted hole/electron transfer mechanism as the dominant path for the formation of the charge-separated state D^+-An-A^-. Geometrical and structural modifications are applied to the bridge units to find an optimal balance between thermodynamics and electronic coupling requirements for a fast unidirectional

dx.doi.org/10.1021/jp505105a | J. Phys. Chem. C 2014, 118, 15600−15609

charge transfer. The results lead to the design of the **1-b_Linear** triad, for which ultrafast charge separation is predicted.

2. METHODS AND COMPUTATIONAL DETAILS

2.1. Ground-State Calculations. To optimize the ground-state geometries of each monomer, dyad, and triad presented in this work, we make use of the ADF software package.[25−27] The geometries are optimized at the B3LYP/TZP level of theory in a dichloromethane (DCM) environment described by the continuum solvent model COSMO.[28] van der Waals dispersion interactions are included using the Grimme3-BJDAMP correction.[29]

2.2. Time-Dependent DFT. Time-Dependent DFT (TD-DFT) is used to calculate the absorption spectra of the investigated systems and to check how the optical properties of the singular components are affected by the assembling into the triad complexes. Several exchange-correlation functionals available in the ADF computational package have been used to check the accuracy of our results in comparison with available experimental data (see Results and Discussion section 3.1).

2.3. Ground- and Excited-State Redox Potentials. ADF is used for the calculation of the ground- and excited-state oxidation potentials of the donor, antenna, and acceptor monomers. Following the procedure described by De Angelis et al.,[30] the ground-state oxidation potential is estimated as

$$G_{ox}^{GS} = G_{sol}^{0} - G_{sol}^{+} \quad (1)$$

Both G_{sol}^{0} and G_{sol}^{+} are obtained by adding the solvent effect to the energies of the molecules optimized in vacuum. The solvent contribution is estimated as the energy difference between the system in solution and in vacuum, calculated at the geometry optimized in solution.

The excited state oxidation potential G_{ox}^{ES} is obtained by subtracting from G_{ox}^{GS} the adiabatic lowest transition energy (E_{0-0})

$$G_{ox}^{ES} = G_{ox}^{GS} - E_{0-0} \quad (2)$$

where E_{0-0} is the energy difference between the excited and the ground states at their corresponding optimized geometries. Results were validated also by calculating the ground-state oxidation potentials using the ΔSCF and Born−Haber cycle methods[31] (Table S2, Supporting Information).

2.4. Excited-State Geometry Optimizations. To investigate the possible electronic relaxations that can occur after photoabsorption, we optimize, for each charge separator, the (i) excitonic state, denoted throughout the paper as S0, in which both the hole and electron are localized on the antenna; (ii) the full charge-separated (CS) state S1 in which the hole is on the donor and the electron on the acceptor; and (iii) the intermediate CS state S2 in which only the hole moves on the donor and the electron stays on the antenna. Other excited states have been investigated, but they all turned out to be much higher in energy, indicating that their formation is strongly unlikely upon visible-light absorption. For each complex, starting from their ground-state optimized geometry, we initially induce a specific optical transition from the ground state to the diabatic state of interest, and subsequently we optimize the geometry of such an excited state. To overcome the systematic underestimation of the excitation energies associated with strong molecular charge transfer character shown by most xc-functionals,[32] we make use of the long-range corrected functional CAM-B3LYP,[33] which has been shown to be quite accurate in describing this type of electronic excitations.[34,35] These calculations are performed using the Gaussian 09 program package[36] using the cc-pVDZ basis set and the polarizable continuum model to simulate the DCM solvation.[37]

2.5. Electronic Coupling and Charge-Separation Rate Calculations. To avoid confusion with the use of the terms donor and acceptor recurring in other sections, we need to specify that when describing hole transfer processes with the term donor we refer to the phenothiazine subunit and with acceptor to the antenna NDI_1. On the other hand, for the electron transfer calculations the terms donor and acceptor have to be intended as the subunits NDI_1 and NDI_2, respectively.

The coupling strength between the orbitals involved in the hole/electron transfer processes is estimated using both the charge transfer integrals (CTI) method implemented in ADF[38−40] and the constrained DFT (CDFT) computational scheme[41−43] implemented in the software package CPMD.[44]

2.5.1. CTI Method (ADF). This formalism computes the CTI through the equation

$$V_{da} = J_{da} - \frac{1}{2}S_{da}(e_d + e_a) \quad (3)$$

Here, J_{da} represents the off-diagonal elements of the Fock matrix constructed using the HOMOs (for hole transfer calculations) or the LUMOs (for electron transfer) of the molecular subunits used as donor (d) or acceptor (a). S_{da} is the overlap integral between the molecular orbitals of the two states considered, while e_d and e_a are the energies of the system bearing the electron/hole on the donor or the acceptor. These calculations are performed at the B3LYP/TZP level in dichloromethane simulated through the continuum solvation model COSMO.

2.5.2. Constrained DFT (CPMD). This methodology is based on the idea of minimizing the Kohn−Sham energy functional under the constraint that the charge difference between two defined regions of space is equal to a specific value of interest n_c. Within the CPMD implementation, we can define these two regions of space as the sum of the atoms constituting, respectively, the donor and the acceptor. For the process of hole transfer, we consider the subsystem PTZ−phenyl−NDI_1 in its linear configuration. Here, PTZ and the phenyl bridge (Ph) form the donor, and NDI_1 forms the acceptor. The electronic coupling is calculated between the two states donor$^+$−acceptor and donor−acceptor$^+$. Similarly, the electron coupling between NDI_1 and NDI_2 is estimated as the coupling between the two states NDI_1^-−bridge−NDI_2 and NDI_1−bridge−NDI_2^-. For the bridge unit we consider either a phenyl ring or an ethyne group; in this case the bridge is not included either in the definition of donor or in the acceptor. The CDFT calculations are performed in vacuum using the pseudopotentials of ref 45 with a plane-wave cutoff of 70 Ry.

As explained in more detail later (section 3.4), depending on the structure of the triad considered, the process of hole transfer between the donor and acceptor can proceed either via a tunneling or via a hopping mechanism. In contrast, the electronic relaxation from NDI_1 to NDI_2 occurs as bridge-mediated electron tunneling for every system investigated. For those cases in which charge transfer occurs through a tunneling mechanism, the overall donor−acceptor coupling is calculated following the McConnel formalism[46]

$$H_{DA} = \frac{h_{Db}}{\Delta\varepsilon}\left(\frac{h_{bb}}{\Delta\varepsilon}\right)^{n-1} h_{bA} \quad (4)$$

dx.doi.org/10.1021/jp505105a | J. Phys. Chem. C 2014, 118, 15600−15609

In eq 4, h_{Db}, h_{bA}, and h_{bb} represent the coupling between a bridge unit and, respectively, the donor, the acceptor, and another bridge unit (if present). The other parameter, $\Delta\varepsilon$, represents the tunneling energy gap imposed by the bridge. $\Delta\varepsilon$ is estimated as the energy difference between the HOMOs (LUMOs) of the hole−(electron)−donor and the bridge. We have verified that this method provides $\Delta\varepsilon$ values very similar to those calculated with the computationally more expensive CDFT method by constraining the charge over the bridge.

3. RESULTS AND DISCUSSION

We initially present in section 3.1 the results of the TD-DFT analysis performed on a series of molecules used as a benchmark to assess the quality of the results given by different GGA and hybrid xc-functionals, in reproducing the experimental absorption spectra published by Matile et al.[19] This analysis is useful to understand the level of theory required to accurately describe the optical response of our triads to their initial photoexcitation.

An accurate calculation of the ground- and excited-state oxidation potentials of the chosen molecular subunits is essential to verify that the donor, antenna, and acceptor moieties do indeed create the redox gradient required for the unidirectional charge transfer. In section 3.2, we compare the computed redox values obtained using the method described in section 2.3, with the experimental cyclic voltammetry data.

In sections 3.3 and 3.4, we extend the TD-DFT study of molecular optical properties to a set of triads on which we apply specific structural changes. We study how these modifications affect the energetics of each excited state by TD-DFT geometry optimization. Starting from the systems showing the most promising thermodynamics we further modify the molecular structure to optimize also the electron coupling between the donor, antenna, and acceptor. Finally, for the optimized molecular rectifier we estimate the charge separation rate constant.

3.1. xc-Functional Benchmarking for TD-DFT Absorption Spectra. TD-DFT studies are performed on the benchmark compounds NDI_1, NDI_2, and NDI_0[16,19,20] making use of the exchange-correlation (xc) functionals OPBE,[47] SAOP,[48,49] OPBE0,[50] B3LYP,[51] and M06.[52,53]

In Table S1 (Supporting Information) we compare the calculated and the experimental values of the first characteristic absorption peak of each molecule investigated. These results clearly indicate that hybrid and meta-hybrid functionals (B3LYP, OPBE0, and M06) are able to predict the lowest excitation energies of the benchmark molecules with much higher accuracy compared to the GGA functional OPBE[47] and the model potential SAOP,[48,49] which considerably underestimate the experimental values. In particular, for the antenna complex NDI_1 used in our triads, the hybrid B3LYP gives a value within 0.1 eV from the experiment.

3.2. Redox Potential Calculations. To verify the presence of a potential gradient between the donor, the antenna, and the acceptor suitable to induce charge separation, we compute the ground- and excited-state redox potentials of each subunit following the procedure described in section 2.3. As shown in Table 1, the redox values calculated at the B3LYP/DCM (COSMO) level compare well with the experimental cyclic voltammetry onset values.[19,20,23] These results overall confirm the validity of the applied method and computational setup. Considering also the positive results obtained with TD-DFT, the choice of the hybrid B3LYP functional appears to be appropriate for studying the electronic and optical properties of molecular complexes employing these functional subunits.

Table 1. Ground (ΔG_{ox}) and Excited State (ΔG_{ox}^{ES}) Molecular Redox Potentials Estimated for Each Molecular Component of the Triad

molecule	redox pot.	$^{a}E_{exp}$ (eV)	$^{b}E_{calc}$ (eV)
NDI_1	ΔG_{ox}	−6.16[19]	−6.21
	ΔG_{ox}^{ES}	−3.82[19]	−3.68
NDI_2	ΔG_{ox}	−7.50[20]	−7.53
	ΔG_{ox}^{ES}	−4.50[20]	−4.60
PTZ	ΔG_{ox}	−4.77[23]	−4.86

[a]Experimental onset redox potentials (measured in dichloromethane). [b]Redox potential values computed using the B3LYP xc-functional in the DCM (COSMO) model. All data are reported vs vacuum.

3.3. Optical Excitations and Excited-State Geometrical Optimizations. The electronic structure of triad **0** is obtained at the ground-state geometry after optimization in dichloromethane, for consistency with the redox potential calculations. The frontier orbitals are depicted in Figure 2.

As expected from the ground- and excited-state oxidation potential calculations, the highest occupied (HOMO) and the lowest unoccupied (LUMO) molecular orbitals are highly localized on the donor and the acceptor, respectively, while the HOMO−1 and the LUMO+1 reside on the antenna. Each of these four orbitals possess the same symmetry of those involved in the main excitation of the subunits calculated separately. The absorption spectrum calculated for triad **0** (Figure 3) shows a dominant peak around 500 nm corresponding to the photoinitiated HOMO−1 to LUMO+1 transition. Figure 3 shows for comparison also the spectra computed for the monomers NDI_1 and NDI_2. The most noticeable difference between these spectra is represented by a 18 nm (0.04 eV) red shift of the first absorption peak of triad **0** with respect to that of the isolated NDI_1. A similar shift is observed for the absorption spectra estimated using different functionals (see Table S3 and Figure S4 in Supporting Information). This red-shift reveals the influence of the substituents in the imide core on the transition energy of the antenna.

The differences between the excited-state oxidation potentials of NDI_1 and NDI_2, as well as between the ground-state potentials of PTZ and NDI_1 (Table 1), imply the presence of driving forces across the linking motifs that represent tunneling barriers separating the components of the triad. Consequently, photoexcitation of the antenna creates the thermodynamic conditions for the exothermic formation of a full charge-separated state where the photogenerated positive hole and the excited electron are localized, respectively, on the donor and the acceptor. Charge separation between the donor and antenna is expected to occur primarily as a hole rather than as an electron transfer process since the tunneling barrier imposed by the bridge is considerably smaller for the first process. Instead, charge separation between the antenna and acceptor will take place through electron tunneling.

To investigate how structural changes can influence the probability of formation of different excited states after photoabsorption, we performed TD-DFT geometry optimizations in the electronic states S0, S1, and S2, for each of the aforementioned systems. The geometrical parameters of the systems optimized for different excited states are summarized in Table S5 of the Supporting Information. For all the investigated cases we observe that in its neutral state the phenothiazine is bent around the N−S axis with an angle of ∼146.8°, while after oxidation (excited states S1 and S2), the molecule assumes a fully planar configuration. This indicates that this particular degree of freedom can be associated with the process of charge transfer

dx.doi.org/10.1021/jp505105a | J. Phys. Chem. C 2014, 118, 15600−15609

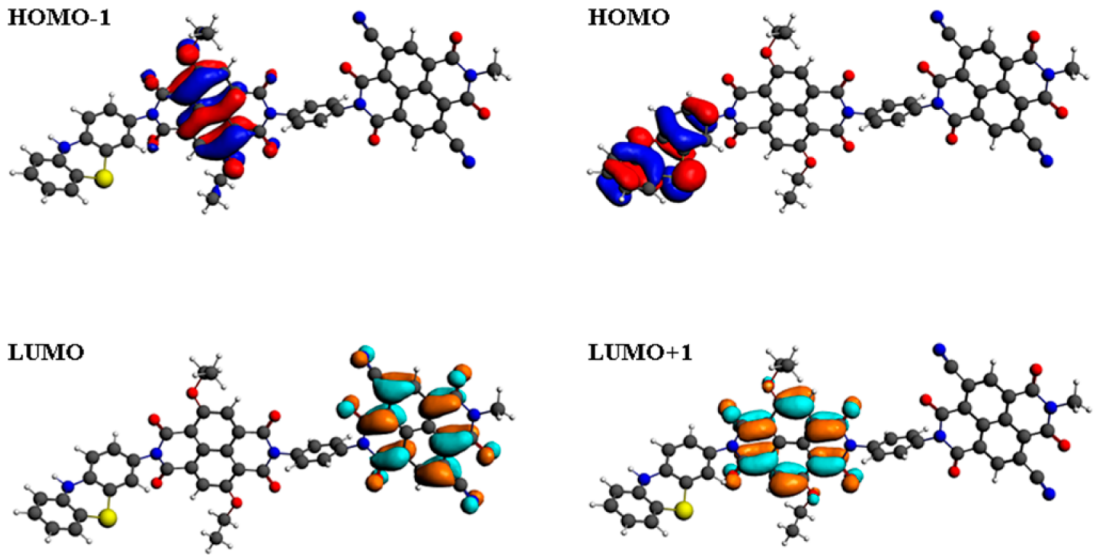

Figure 2. Frontier molecular orbitals of triad **0** obtained at the B3LYP/TZP level of theory in DCM solvent.

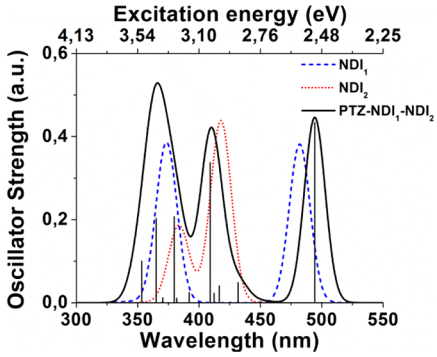

Figure 3. Optical absorption spectra computed with TD-DFT for NDI_1 (blue dashes), for NDI_2 (red dots), and for the whole triad system **0** (black curve). The black solid lines represent the calculated excitations contributing to the absorption spectra of system **0**. TD-DFT calculations are performed in DCM (COSMO) using the B3LYP/TZP level of theory with ADF.

between the donor and antenna. Moreover, we observe that the dihedral angle between the PTZ and the directly bound phenyl bridge assumes different values depending on the configuration of PTZ: When PTZ is in a perpendicular configuration (see Figure 1) this angle is close to 90°, while for PTZ in the linear configuration it is found to be ∼36°, which is consistent with previously studied systems containing phenyl bridges.[54] As discussed later, variation of this torsional angle has an important effect on the relative stability of different excited states.

We also observe that optimization in S0 does not lead to any major geometrical change compared to the ground state, independently of the rectifier considered. The maximum energy difference (evaluated at the ground-state PES) between the geometries optimized in the ground and the excitonic states is ∼0.01 eV, which is at least 1 order of magnitude smaller than the difference calculated for the geometries optimized in any other excited state. Therefore, we use the energy minimum of S0 as a reference point to appreciate how the energies of S1 and S2 are affected by structural modifications.

The free energy change upon charge separation can be estimated as

$$\Delta G = \mathrm{IE} - \mathrm{EA} - 1/r_{\mathrm{D-A}} \qquad (5)$$

In eq 5, IE and EA represent the ionization potential and electron affinity of the donor and the acceptor systems, respectively, while $r_{\mathrm{D-A}}$ is the distance between the donor and acceptor. By increasing the distance $r_{\mathrm{D-A}}$ by means of a bridge, due to the Coulomb term we expect a progressive destabilization of the charge-separated states induced by drifting the positive and negative charges apart; to a first approximation we can assume that IE and EA remain constant for systems of the same group (presenting a linear or perpendicular arrangement of PTZ).

Figure 4 and Table 2 show the comparison between the PESs obtained through excited-state geometry optimizations of the different charge separators. The first thing to notice in Table 2 is that for system **0** the two states S1 and S2 are both thermodynamically accessible from S0, but there is no driving force from S2 to the fully CS state S1. The insertion of a phenyl bridge between PTZ and NDI_1 has a destabilizing effect for the intermediate state S2, in both the linear and perpendicular triads (system **1_Linear** and system **1_Perperpendicular** in Figure 4). This effect is further enhanced by adding a second phenyl bridge (see system **2_Linear** and system **2_Perperpendicular** in Figure 4). In Table 2 we can see how the $\Delta G(\mathrm{S2-S0})$ changes by changing the distance between donor and acceptor subunits. This effect follows the expected dependence of ΔG on $r_{\mathrm{D-A}}$. In particular, if we plot the minimum energy of the intermediate CS state S2 against the donor−antenna distance, we observe that the destabilization of S2 is linearly dependent on the number of bridge units introduced. The destabilization per ring is equivalent to 0.35 eV for the linear systems and to 0.30 eV for the perpendicular ones (see Figure S6 in Supporting Information). In the absence of a bridge, the CS state S2 is energetically very similar to the fully CS state S1. This suggests that in S1 the larger electron affinity of the acceptor (NDI_2) compensates the destabilization factor derived by a larger hole−electron distance compared to the state S2.

If we look at the behavior of S1 we notice that the insertion of phenyl units does not affect significantly the energy of the S1 minimum with respect to the ground state. In Table 2 we observe that the insertion of a first phenyl ring does not lead to any relevant variation of $\Delta G(\mathrm{S1-S0})$. The insertion of a second ring reduces the thermodynamic force with respect to the excitonic state, especially for the linear case. This effect appears to be

dx.doi.org/10.1021/jp505105a | J. Phys. Chem. C 2014, 118, 15600−15609

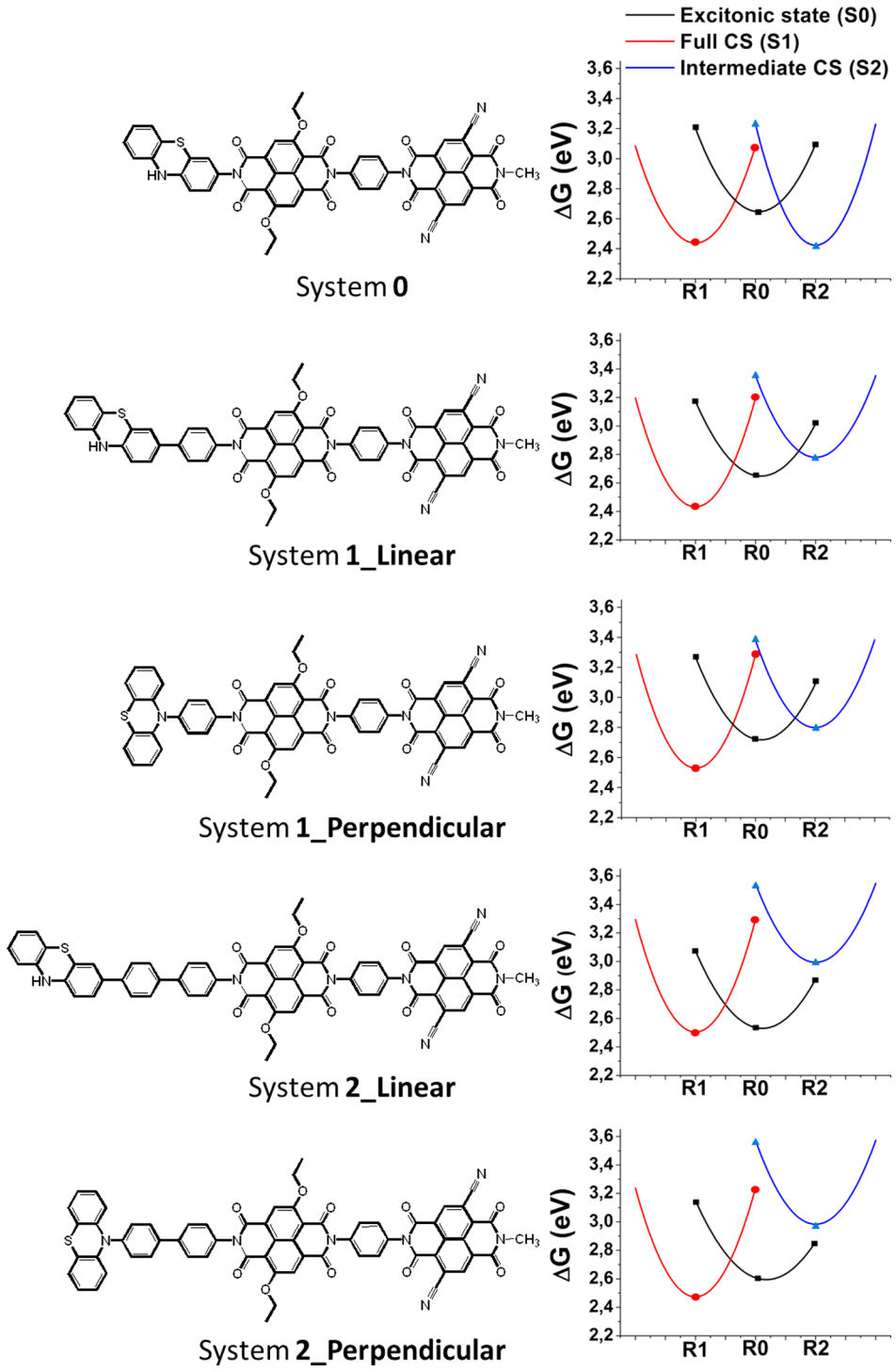

Figure 4. Potential energy surfaces for the antenna-localized exciton state S0 (black), the fully charge-separated state S1 (red), and the intermediate charge-separated state (representing the hole displacement from An to D) S2 (blue). The energies are obtained with TD-DFT geometry optimizations at the CAM-B3LYP/cc-pVDZ level and reported vs the minimal energy of the ground state along a nuclear collective coordinate R. R0, R1, and R2 represent the geometries optimized for each excited state. The symbols along the curves represent the energy values used for the construction of the parabolas and the calculation of the reorganization energies λ and energy difference ΔG (here we neglect the entropic and zero-point energy contributions which we assume to be small compared to ΔE).

induced mostly by a shift of the energy minimum of S0. It should be noticed that for the S1 state the distance between the hole and the electron is quite large (around 20 Å), and thus the Coulomb term is no longer the dominant factor in determining the ΔG.

Overall, these results indicate that system **1** is the best choice for the optimization of the thermodynamic force toward the full charge-separated state. The presence of one bridge unit dividing the donor and the antenna induces the optimal thermodynamic conditions that favor the formation of S1 over the alternative S2 and S0 states. The S1 state is expected to be formed by a concerted transfer of a hole from the antenna to the donor and an electron from the antenna toward the acceptor. In the following section 3.4 the reasons for a preference between the perpendicular or the linear geometry for system **1** are discussed.

dx.doi.org/10.1021/jp505105a | J. Phys. Chem. C 2014, 118, 15600−15609

Table 2. Minimal Energy Differences between Excited-State PES and Reorganization Energies Calculated for the Investigated Systems[a]

	S1−S0		S2−S0		S1−S2	
	ΔG (eV)	λ (eV)	ΔG (eV)	λ (eV)	ΔG (eV)	λ (eV)
System **0**	−0.21	0.65	−0.22	0.80	0.014	0.41
System **1 Linear**	−0.22	0.76	0.13	0.57	−0.35	0.40
System **1 Perpendicular**	−0.19	0.75	0.08	0.58	−0.27	0.38
System **2 Linear**	−0.031	0.79	0.46	0.55	−0.49	0.39
System **2 Perpendicular**	−0.13	0.76	0.38	0.59	−0.51	0.50

[a]ΔG values are calculated as the energy difference between the minima of the different excited state PESs (S*n*−S*m*) obtained through TD-DFT geometry optimization at the CAM-B3LYP/cc-pVDZ level of theory. λ is the reorganization energy calculated along the S*n* energy surface.

3.4. Charge Transfer Integrals and Charge Separation Rates. So far our analysis has been focused on the effects that structural changes have on the energy gradients between different excited states. However, to assess the charge separation efficiency of a particular triad we cannot limit our analysis solely to the system's thermodynamics. Indeed, although Marcus[55] theory (eq 6) defines the electron-transfer rate constant (k_{ET}) between two electronic states as directly dependent on their Gibbs free energy difference (ΔG)

$$k_{ET} = \frac{2\pi}{\hbar}\frac{2}{\sqrt{4\pi\lambda k_B T}}|H_{DA}|^2 \exp\left(-\frac{(\Delta G + \lambda)^2}{4\lambda k_B T}\right) \quad (6)$$

the probability of this process to occur is strictly correlated also to the electron coupling term (H_{DA}), which measures the overlap between the orbitals dominating those two electronic states. For systems in which the donor and the acceptor are not directly in contact, their coupling strongly depends on the nature of their connecting bridge, which also defines whether the transfer occurs via electron tunneling or a bridge-mediated charge hopping mechanism. In the first case the transfer rate is strongly distance dependent, and H_{DA} is a function of the tunneling barrier height imposed by the bridge. In the other case, its energy levels can be thermodynamically accessed by the moving charges, and therefore it no longer constitutes a barrier.[56]

Table 3 summarizes the electronic coupling between the different subunits calculated for both the linear and perpendicular system **1** using both the CTI and CDFT methods.

Table 3. Comparison between the Coupling Values for Hole and Electron Transfer, Estimated via CTI and Constrained DFT Methods[a]

	$^{CTI}H_{DA}$ (meV)	Δε (meV)	$^{CDFT}H_{DA}$ (meV)
PTZ−Ph−NDI$_1$ (L)	8	-	3
PTZ−Ph−NDI$_1$ (P)	0.3	1000[a]	-
NDI$_1$−Ph−NDI$_2$	0.04	2400[b]	0.05
NDI$_1$−C≡C−NDI$_2$	23	820[b]	43.5

[a]CTI: Electron/hole coupling values calculated for the dyads listed in the first column. (L) and (P) indicate the linear or perpendicular position of phenothiazine with respect to the phenyl bridge (Ph). Calculations are performed with ADF at the B3LYP/TZP level of theory in DCM (COSMO). The same computational setup is used to calculate Δε, which represents the energy difference between the HOMOs (a) or the LUMOs (b) of NDI$_1$ and Ph. These values are used in the McConnel's formalism to calculate $^{CTI}H_{DA}$ values. Similar values are obtained using the CDFT approach (not shown). CDFT: coupling values obtained employing the constrained DFT method implemented in the CPMD package; the CDFT calculations are performed in vacuum, using the BLYP functional and a plane wave cutoff of 70 Ry.

The orbital analyses of system **1** in its linear and perpendicular geometries show highly localized frontier molecular orbitals that strongly resemble those already discussed for system **0**. The only difference is represented by the HOMO of system **1_Linear**, which appears to be delocalized over both the PTZ and the phenyl bridge, indicating that the bridge no longer constitutes a barrier in the process of hole transfer between the antenna and the electron donor. When PTZ is perpendicular to Ph, the delocalization is not observed. Therefore, in this case the hole is expected to move from the antenna to the donor by tunneling through the energy barrier imposed by Ph. No delocalization is observed also for the LUMO and the LUMO+1, for any of the analyzed systems. Electron transfer between the antenna and acceptor should therefore occur as well via electron tunneling.

To calculate the coupling between the electronic states involved in the formation of the charge-separated state S1, we study separately the donor−bridge−antenna (hole transfer) and antenna−bridge−acceptor (electron transfer) subsystems listed in Table 3. The group NDI$_1$−C≡C−NDI$_2$ is added to the list to decrease the electron tunneling energy barrier height imposed by the bridge and allow for rotation between the two naphthalene diimides.

We can immediately notice how CTI and CDFT formalisms give comparable results despite the different level of theory and environment conditions applied. This gives some confidence in the estimation of the tunneling barrier.

More importantly, the results shown in Table 3 highlight the large effect of having PTZ linked to the phenyl bridge in a linear or a perpendicular fashion: The electronic coupling between the hole donor (NDI$_1$) and the acceptor (PTZ) differs by more than 1 order of magnitude between the two systems. The cause of this difference is attributed to the large hole-transfer barrier (1 eV) imposed by the phenyl ring in the perpendicular configuration, which disappears in the linear system due to the delocalization of the HOMO over both the PTZ and the bridge.

Even a larger barrier (2.4 eV) is induced by Ph for the electron tunneling between NDI$_1$ and NDI$_2$, reducing the electronic coupling between the two practically to zero. The substitution of the Ph bridge with an acetylene group leads to an increase of the antenna−acceptor electron coupling of 4 orders of magnitude (Table 3). By applying this latter change to the structure of system **1_Linear**, we obtain system **1-b_Linear** shown in Figure 5. Table 4 shows the thermodynamic and electronic coupling values computed for this triad. As expected, we observe that S1 is the energetically most stable excited state, with $\Delta G = -0.26$ eV with respect to S0, while the formation of any other competing electronic state appears thermodynamically unfavorable.

Since the formation of the charge-separated state S1 is expected to take place as a concerted hole and electron

dx.doi.org/10.1021/jp505105a | J. Phys. Chem. C 2014, 118, 15600−15609

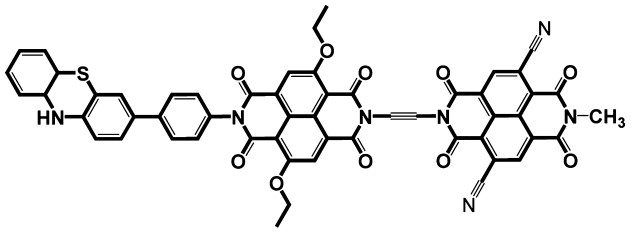

Figure 5. Schematic representation of the molecular rectifier **1-b_Linear** optimized for ultrafast formation of the charge-separated state S1.

Table 4. Thermodynamic Driving Force ΔG and Electronic Coupling Values Computed for the Triad 1-b_Linear, Respectively, at the CAM-B3LYP and B3LYP Levels

	S1−S0		S2−S0		electron coupling	
	ΔG (eV)	λ (eV)	ΔG (eV)	λ (eV)	$H_{D\text{-}An}$ (meV)	$H_{An\text{-}A}$ (meV)
1-b_Linear	−0.26	0.70	0.10	0.90	8	23

displacement from the antenna toward, respectively, the donor and the acceptor units, we can reasonably assume that the kinetic bottleneck for this process is represented by the oxidation of PTZ due to the weaker electronic coupling with NDI_1. Under this assumption, we can employ eq 6 to estimate the rate of formation for S1. By using the values H_{DA} = 0.008 eV, ΔG = −0.26 eV, and λ = 0.7 eV, we obtain a rate constant $k_{ET} = 1.24 \times 10^{12}$ s^{-1}, which is similar to the rate of 5×10^{12} s^{-1} experimentally observed for the process of hole transfer between a perylene and a phenothiazine linked through a *p*-phenylene oligomer.[54]

4. CONCLUSIONS

With the goal of obtaining a molecular triad able to induce a stable charge-separated state upon visible-light absorption, we design several complexes employing PTZ, NDI_1, and NDI_2, respectively, as electron donor, antenna, and electron acceptor, using different linkages between these subunits. The investigation of the optical properties performed for each triad reveals a predominant $\pi-\pi^*$ excitation around 500 nm associated with the antenna-localized excited state S0. The relative energetic stability of this initial excited state with respect to the excited states with charge transfer character is found to be dependent on the donor−antenna distance. The separation of these two moieties by means of one phenyl ring appears to be the optimal compromise to ensure a strong driving force for the formation of the fully charge-separated state S1 starting from S0 and prevent the occurrence of competing quenching paths for the excitonic state.

It is found that a strong coupling between the donor and antenna is achieved when the PTZ is linked to the phenyl bridge through one of its peripheral aromatic rings. At the same time the ethyne group is shown to provide a strong electronic coupling between the antenna and the acceptor moieties.

On the basis of these findings, we propose the molecular rectifier PTZ−Ph−NDI_1−C≡C−NDI_2 as a promising triad for photoinduced direct ultrafast charge separation. Recombination of the photoinduced CS state to the ground state is expected to be strongly delayed due to the long distance and large energy barrier between the donor and acceptor imposed by the other molecular components. Additionally, in an ensemble where multiple rectifiers are stacked through $\pi-\pi$ interactions, the n-type semiconductor behavior of NDI_2 will have two major advantages: it will further delay charge recombination by delocalizing the electron in the bulk and allow the creation of a p−n junction with a suitable electrode such as silicon. The next steps currently under investigation are a more comprehensive description of the dynamical effect associated with the ET process and the substitution of the electron donor with a water oxidation catalyst to develop a genuine artificial photosynthesis device.

■ ASSOCIATED CONTENT

Supporting Information

Comparison between ground-state oxidation potentials evaluated for PTZ, NDI_1, and NDI_2 with different methods. Comparison between absorption spectra calculated with different xc-functionals for system **0** in dichloromethane. Geometrical parameters of the investigated systems optimized in the ground and excited states. Graphical representation of the dependence of ΔG (S2−S0) on the D−An distance. This material is available free of charge via the Internet at http://pubs.acs.org.

■ AUTHOR INFORMATION

Corresponding Author

*E-mail: f.buda@chem.leidenuniv.nl.

Notes

The authors declare no competing financial interest.

■ ACKNOWLEDGMENTS

The use of supercomputer facilities was sponsored by NWO Physical Sciences, with financial support from The Netherlands Organization for Scientific Research (NWO). This research is financed by the NWO-ECHO project number 713.011.002 and by the BioSolarCells open innovation consortium, supported by the Dutch Ministry of Economic Affairs, Agriculture and Innovation (project C1.9).

■ REFERENCES

(1) Young, K. J.; Martini, L. A.; Milot, R. L.; Snoeberger, R. C., III; Batista, V. S.; Schmuttenmaer, C. A.; Crabtree, R. H.; Brudvig, G. W. Light-Driven Water Oxidation for Solar Fuels. *Coord. Chem. Rev.* **2012**, *256*, 2503−2520.

(2) Xiao, D.; Martini, L. A.; Snoeberger, R. C.; Crabtree, R. H.; Batista, V. S. Inverse Design and Synthesis of Acac-Coumarin Anchors for Robust TiO2 Sensitization. *J. Am. Chem. Soc.* **2011**, *133*, 9014−9022.

(3) Negre, C. F. A.; Milot, R. L.; Martini, L. A.; Ding, W.; Crabtree, R. H.; Schmuttenmaer, C. A.; Batista, V. S. Efficiency of Interfacial Electron Transfer from Zn-Porphyrin Dyes into TiO2 Correlated to the Linker Single Molecule Conductance. *J. Phys. Chem. C* **2013**, *117*, 24462−24470.

(4) Martini, L. A.; Moore, G. F.; Milot, R. L.; Cai, L. Z.; Sheehan, S. W.; Schmuttenmaer, C. A.; Brudvig, G. W.; Crabtree, R. H. Modular Assembly of High-Potential Zinc Porphyrin Photosensitizers Attached to TiO2 with a Series of Anchoring Groups. *J. Phys. Chem. C* **2013**, *117*, 14526−14533.

(5) Akimov, A. V.; Neukirch, A. J.; Prezhdo, O. V. Theoretical Insights into Photoinduced Charge Transfer and Catalysis at Oxide Interfaces. *Chem. Rev.* **2013**, *113*, 4496−4565.

(6) Faunce, T.; Styring, S.; Wasielewski, M. R.; Brudvig, G. W.; Rutherford, A. W.; Messinger, J.; Lee, A. F.; Hill, C. L.; deGroot, H.; Fontecave, M.; et al. Artificial Photosynthesis as a Frontier Technology for Energy Sustainability. *Energy Environ. Sci.* **2013**, *6*, 1074−1076.

(7) Yu, M.-L.; Wang, S.-M.; Feng, K.; Khoury, T.; Crossley, M. J.; Yang, F.; Zhang, J.-P.; Tung, C.-H.; Wu, L.-Z. Photoinduced Electron Transfer and Charge-Recombination in 2-Ureido-4[1H]-Pyrimidinone Quadruple Hydrogen-Bonded Porphyrin−Fullerene Assemblies. *J. Phys. Chem. C* **2011**, *115*, 23634−23641.

(8) Wenger, O. S. Long-Range Electron Transfer in Artificial Systems with d6 and d8Metal Photosensitizers. *Coord. Chem. Rev.* **2009**, *253*, 1439−1457.
(9) Hankache, J.; Niemi, M.; Lemmetyinen, H.; Wenger, O. S. Hydrogen-Bonding Effects on the Formation and Lifetimes of Charge-Separated States in Molecular Triads. *J. Phys. Chem. A* **2012**, *116*, 8159−8168.
(10) Gust, D.; Moore, T. A.; Moore, A. L. Solar Fuels via Artificial Photosynthesis. *Acc. Chem. Res.* **2009**, *42*, 1890−1898.
(11) Andrea Rozzi, C.; Maria Falke, S.; Spallanzani, N.; Rubio, A.; Molinari, E.; Brida, D.; Maiuri, M.; Cerullo, G.; Schramm, H.; Christoffers, J.; et al. Quantum Coherence Controls the Charge Separation in a Prototypical Artificial Light-Harvesting System. *Nat. Commun.* **2013**, *4*, 1602.
(12) Yella, A.; Lee, H.-W.; Tsao, H. N.; Yi, C.; Chandiran, A. K.; Nazeeruddin, M. K.; Diau, E. W.-G.; Yeh, C.-Y.; Zakeeruddin, S. M.; Grätzel, M. Porphyrin-Sensitized Solar Cells with Cobalt (II/III)−Based Redox Electrolyte Exceed 12% Efficiency. *Science* **2011**, *334*, 629−634.
(13) Megiatto, J. D., Jr; Méndez-Hernández, D. D.; Tejeda-Ferrari, M. E.; Teillout, A.-L.; Llansola-Portolés, M. J.; Kodis, G.; Poluektov, O. G.; Rajh, T.; Mujica, V.; Groy, T. L.; et al. A Bioinspired Redox Relay That Mimics Radical Interactions of the Tyr−His Pairs of Photosystem II. *Nat. Chem.* **2014**, *6*, 423−428.
(14) Nattestad, A.; Mozer, A. J.; Fischer, M. K. R.; Cheng, Y.-B.; Mishra, A.; Bäuerle, P.; Bach, U. Highly Efficient Photocathodes for Dye-Sensitized Tandem Solar Cells. *Nat. Mater.* **2010**, *9*, 31−35.
(15) Listorti, A.; O'Regan, B.; Durrant, J. R. Electron Transfer Dynamics in Dye-Sensitized Solar Cells. *Chem. Mater.* **2011**, *23*, 3381−3399.
(16) Suraru, S.-L.; Würthner, F. Core-Tetrasubstituted Naphthalene Diimides by Stille Cross-Coupling Reactions and Characterization of Their Optical and Redox Properties. *Synthesis* **2009**, *2009*, 1841−1845.
(17) Supur, M.; El-Khouly, M. E.; Seok, J. H.; Kay, K.-Y.; Fukuzumi, S. Elongation of Lifetime of the Charge-Separated State of Ferrocene−Naphthalenediimide−[60]Fullerene Triad via Stepwise Electron Transfer. *J. Phys. Chem. A* **2011**, *115*, 14430−14437.
(18) Steyrleuthner, R.; Schubert, M.; Howard, I.; Klaumünzer, B.; Schilling, K.; Chen, Z.; Saalfrank, P.; Laquai, F.; Facchetti, A.; Neher, D. Aggregation in a High-Mobility N-Type Low-Bandgap Copolymer with Implications on Semicrystalline Morphology. *J. Am. Chem. Soc.* **2012**, *134*, 18303−18317.
(19) Kishore, R. S. K.; Kel, O.; Banerji, N.; Emery, D.; Bollot, G.; Mareda, J.; Gomez-Casado, A.; Jonkheijm, P.; Huskens, J.; Maroni, P.; et al. Ordered and Oriented Supramolecular N/p-Heterojunction Surface Architectures: Completion of the Primary Color Collection. *J. Am. Chem. Soc.* **2009**, *131*, 11106−11116.
(20) Sakai, N.; Mareda, J.; Vauthey, E.; Matile, S. Core-Substituted Naphthalenediimides. *Chem. Commun.* **2010**, *46*, 4225−4237.
(21) Bhosale, S. V.; Jani, C. H.; Langford, S. J. Chemistry of Naphthalene Diimides. *Chem. Soc. Rev.* **2008**, *37*, 331.
(22) Jones, B. A.; Facchetti, A.; Marks, T. J.; Wasielewski, M. R. Cyanonaphthalene Diimide Semiconductors for Air-Stable, Flexible, and Optically Transparent N-Channel Field-Effect Transistors. *Chem. Mater.* **2007**, *19*, 2703−2705.
(23) Gomurashvili, Z.; Crivello, J. V. Phenothiazine Photosensitizers for Onium Salt Photoinitiated Cationic Polymerization. *J. Polym. Sci., Part A: Polym. Chem.* **2001**, *39*, 1187−1197.
(24) Jones, B. A.; Facchetti, A.; Wasielewski, M. R.; Marks, T. J. Tuning Orbital Energetics in Arylene Diimide Semiconductors. Materials Design for Ambient Stability of N-Type Charge Transport. *J. Am. Chem. Soc.* **2007**, *129*, 15259−15278.
(25) Guerra, C. F.; Snijders, J. G.; Velde, G. te; Baerends, E. J. Towards an Order-N DFT Method. *Theor. Chem. Acc.* **1998**, *99*, 391−403.
(26) Te Velde, G.; Bickelhaupt, F. M.; Baerends, E. J.; Fonseca Guerra, C.; van Gisbergen, S. J. A.; Snijders, J. G.; Ziegler, T. Chemistry with ADF. *J. Comput. Chem.* **2001**, *22*, 931−967.
(27) SCM: Required citations - ADF http://www.scm.com/Doc/Doc2012/Background/References/page4.html (accessed Oct 9, 2012).
(28) Pye, C. C.; Ziegler, T. An Implementation of the Conductor-like Screening Model of Solvation within the Amsterdam Density Functional Package. *Theor. Chem. Acc.* **1999**, *101*, 396−408.
(29) Grimme, S.; Antony, J.; Ehrlich, S.; Krieg, H. A Consistent and Accurate Ab Initio Parametrization of Density Functional Dispersion Correction (DFT-D) for the 94 Elements H-Pu. *J. Chem. Phys.* **2010**, *132*, 154104−154104-19.
(30) Pastore, M.; Fantacci, S.; De Angelis, F. Ab Initio Determination of Ground and Excited State Oxidation Potentials of Organic Chromophores for Dye-Sensitized Solar Cells. *J. Phys. Chem. C* **2010**, *114*, 22742−22750.
(31) Wang, T.; Brudvig, G. W.; Batista, V. S. Study of Proton Coupled Electron Transfer in a Biomimetic Dimanganese Water Oxidation Catalyst with Terminal Water Ligands. *J. Chem. Theory Comput.* **2010**, *6*, 2395−2401.
(32) Gritsenko, O.; Baerends, E. J. Asymptotic Correction of the Exchange−correlation Kernel of Time-Dependent Density Functional Theory for Long-Range Charge-Transfer Excitations. *J. Chem. Phys.* **2004**, *121*, 655−660.
(33) Yanai, T.; Tew, D. P.; Handy, N. C. A New Hybrid Exchange−correlation Functional Using the Coulomb-Attenuating Method (CAM-B3LYP). *Chem. Phys. Lett.* **2004**, *393*, 51−57.
(34) Jacquemin, D.; Planchat, A.; Adamo, C.; Mennucci, B. TD-DFT Assessment of Functionals for Optical 0−0 Transitions in Solvated Dyes. *J. Chem. Theory Comput.* **2012**, *8*, 2359−2372.
(35) Tawada, Y.; Tsuneda, T.; Yanagisawa, S.; Yanai, T.; Hirao, K. A Long-Range-Corrected Time-Dependent Density Functional Theory. *J. Chem. Phys.* **2004**, *120*, 8425−8433.
(36) Frisch, M. J.; Trucks, G. W.; Schlegel, H. B.; Scuseria, G. E.; Robb, M. A.; Cheeseman, J. R.; Scalmani, G.; Barone, V.; Mennucci, B.; Petersson, G. A.; Nakatsuji, H.; Caricato, M.; Li, X.; Hratchian, H. P.; Izmaylov, A. F.; Bloino, J.; Zheng, G.; Sonnenberg, J. L.; Hada, M.; Ehara, M.; Toyota, K.; Fukuda, R.; Hasegawa, J.; Ishida, M.; Nakajima, T.; Honda, Y.; Kitao, O.; Nakai, H.; Vreven, T.; Montgomery, J. A., Jr.; Peralta, J. E.; Ogliaro, F.; Bearpark, M.; Heyd, J. J.; Brothers, E.; Kudin, K. N.; Staroverov, V. N.; Kobayashi, R.; Normand, J.; Raghavachari, K.; Rendell, A.; Burant, J. C.; Iyengar, S. S.; Tomasi, J.; Cossi, M.; Rega, N.; Millam, J. M.; Klene, M.; Knox, J. E.; Cross, J. B.; Bakken, V.; Adamo, C.; Jaramillo, J.; Gomperts, R.; Stratmann, R. E.; Yazyev, O.; Austin, A. J.; Cammi, R.; Pomelli, C.; Ochterski, J. W.; Martin, R. L.; Morokuma, K.; Zakrzewski, V. G.; Voth, G. A.; Salvador, P.; Dannenberg, J. J.; Dapprich, S.; Daniels, A. D.; Ö. Farkas, Foresman, J. B.; Ortiz, J. V.; Cioslowski, J.; Fox, D. J. *Gaussian 09*, Revision D.01; Gaussian, Inc.: Wallingford CT, 2009.
(37) Tomasi, J.; Mennucci, B.; Cammi, R. Quantum Mechanical Continuum Solvation Models. *Chem. Rev.* **2005**, *105*, 2999−3093.
(38) Newton, M. D. Quantum Chemical Probes of Electron-Transfer Kinetics: The Nature of Donor-Acceptor Interactions. *Chem. Rev.* **1991**, *91*, 767−792.
(39) Senthilkumar, K.; Grozema, F. C.; Bickelhaupt, F. M.; Siebbeles, L. D. A. Charge Transport in Columnar Stacked Triphenylenes: Effects of Conformational Fluctuations on Charge Transfer Integrals and Site Energies. *J. Chem. Phys.* **2003**, *119*, 9809−9817.
(40) Senthilkumar, K.; Grozema, F. C.; Guerra, C. F.; Bickelhaupt, F. M.; Lewis, F. D.; Berlin, Y. A.; Ratner, M. A.; Siebbeles, L. D. A. Absolute Rates of Hole Transfer in DNA. *J. Am. Chem. Soc.* **2005**, *127*, 14894−14903.
(41) Oberhofer, H.; Blumberger, J. Electronic Coupling Matrix Elements from Charge Constrained Density Functional Theory Calculations Using a Plane Wave Basis Set. *J. Chem. Phys.* **2010**, *133*, 244105−244105−10.
(42) Oberhofer, H.; Blumberger, J. Charge Constrained Density Functional Molecular Dynamics for Simulation of Condensed Phase Electron Transfer Reactions. *J. Chem. Phys.* **2009**, *131*, 064101−064101−11.
(43) Wu, Q.; Voorhis, T. V. Extracting Electron Transfer Coupling Elements from Constrained Density Functional Theory. *J. Chem. Phys.* **2006**, *125*, 164105.

(44) CPMD, http://www.cpmd.org/, *Copyright IBM Corp 1990−2008, Copyright MPI fürFestkörperforschung Stuttgart* 1997−2001.
(45) Goedecker, S.; Teter, M.; Hutter, J. Separable Dual-Space Gaussian Pseudopotentials. *Phys. Rev. B* **1996**, *54*, 1703−1710.
(46) McConnell, H. M. Intramolecular Charge Transfer in Aromatic Free Radicals. *J. Chem. Phys.* **1961**, *35*, 508−515.
(47) Perdew, J. P.; Burke, K.; Ernzerhof, M. Generalized Gradient Approximation Made Simple. *Phys. Rev. Lett.* **1996**, *77*, 3865−3868.
(48) Gritsenko, O. V.; Schipper, P. R. T.; Baerends, E. J. Approximation of the Exchange-Correlation Kohn−Sham Potential with a Statistical Average of Different Orbital Model Potentials. *Chem. Phys. Lett.* **1999**, *302*, 199−207.
(49) Schipper, P. R. T.; Gritsenko, O. V.; van Gisbergen, S. J. A.; Baerends, E. J. Molecular Calculations of Excitation Energies and (hyper)polarizabilities with a Statistical Average of Orbital Model Exchange-Correlation Potentials. *J. Chem. Phys.* **2000**, *112*, 1344−1352.
(50) Swart, M.; Ehlers, A. W.; Lammertsma, K. Performance of the OPBE Exchange-Correlation Functional. *Mol. Phys.* **2004**, *102*, 2467−2474.
(51) Reiher, M.; Salomon, O.; Hess, B. A. Reparameterization of Hybrid Functionals Based on Energy Differences of States of Different Multiplicity. *Theor. Chem. Acc.* **2001**, *107*, 48−55.
(52) Zhao, Y.; Truhlar, D. The M06 Suite of Density Functionals for Main Group Thermochemistry, Thermochemical Kinetics, Noncovalent Interactions, Excited States, and Transition Elements: Two New Functionals and Systematic Testing of Four M06-Class Functionals and 12 Other Functionals. *Theor. Chem. Acc.* **2008**, *120*, 215−241.
(53) Zhao, Y.; Truhlar, D. G. A New Local Density Functional for Main-Group Thermochemistry, Transition Metal Bonding, Thermochemical Kinetics, and Noncovalent Interactions. *J. Chem. Phys.* **2006**, *125*, 194101−194101−18.
(54) Weiss, E. A.; Ahrens, M. J.; Sinks, L. E.; Gusev, A. V.; Ratner, M. A.; Wasielewski, M. R. Making a Molecular Wire: Charge and Spin Transport through Para-Phenylene Oligomers. *J. Am. Chem. Soc.* **2004**, *126*, 5577−5584.
(55) Marcus, R. A. On the Theory of Oxidation-Reduction Reactions Involving Electron Transfer. I. *J. Chem. Phys.* **1956**, *24*, 966−978.
(56) Hanss, D.; Wenger, O. S. Tunneling Barrier Effects on Photoinduced Charge Transfer through Covalent Rigid Rod-Like Bridges. *Inorg. Chem.* **2009**, *48*, 671−680.